

Three-dimensional tomographic reconstruction of ultrashort free electron wave packets

M. Wollenhaupt · M. Krug · J. Köhler · T. Bayer ·
C. Sarpe-Tudoran · T. Baumert

Received: 1 April 2009 / Published online: 19 April 2009
© Springer-Verlag 2009

Abstract We present a tomographic technique based on Photoelectron Angular Distributions (PADs) measured by Velocity-Map-Imaging (VMI) to reconstruct the three-dimensional shape of ultrashort free electron wave packets obtained from 1 + 2 Resonance Enhanced Multi-Photon Ionization (REMPI) of potassium atoms. To this end the laser pulse is rotated about its propagation direction and a set of PADs are recorded at different rotation angles. The tomographic reconstruction technique is described and results for linear and elliptical polarization are presented. Results for linearly polarized light producing cylindrically symmetric electron wave packets confirm the validity of our method whereas elliptically polarized light serves as a prototype for polarization-shaped laser pulses.

PACS 32.80.Qk · 32.80.Rm · 33.80.Rv

1 Introduction

In recent years, quantum control by shaped ultrashort laser pulses has become more and more versatile and effective by utilization of refined experimental techniques. Pulse shaping has become technically mature resulting in compact devices and extended pulse-shaping capabilities [1, 2]. Control exerted by polarization-shaped ultrashort laser pulses in atomic and molecular physics [3–5] has received much

attention because it exploits the three-dimensional character of the light-matter interaction. The development of detection techniques providing highly differential information on a quantum system has proven equally important to investigate controlled dynamics. In quantum control, photoelectron spectroscopy on atoms and molecules in the gas phase plays a prominent role due to its capability to deliver highly detailed information on the light-induced dynamics [6]. Besides control of neutral dynamics, coherent control of ultrashort free electron wave packets has also been studied by photoelectron spectroscopy in an interference experiment [7] demonstrating Young's double-slit in time domain. With the advent of polarization shaping [8] and the associated options for three-dimensional coherent control, detection schemes for three-dimensional observation are in great demand. Fundamental aspects of light-matter interactions have been studied using three-dimensional observation techniques such as Cold Target Recoil Ion Momentum Spectroscopy (COLTRIMS) [9] or tomography by analysis of high order harmonic radiation [10]. Another method to derive three-dimensional (cylindrically symmetrical) distributions via Abel-inversion [11–14] from two-dimensional measurements of Photoelectron Angular Distributions (PADs) [15–18] requires linearly polarized light with the polarization vector parallel to the detector plane. Recently, experiments aiming at the analysis of physical mechanisms underlying strong-field control studied coherent electronic excitation of atoms [19–24]. An extension towards three-dimensional coherent control combining polarization-shaped laser pulses with two-dimensional detection of PADs was carried out [25]. In that work, it was demonstrated by comparison of measured and simulated PADs that polarization shaping delivers a high degree of control on the angular distributions of ultrashort free electron wave packets. In this paper, we generalize the princi-

M. Wollenhaupt (✉) · M. Krug · J. Köhler · T. Bayer ·
C. Sarpe-Tudoran · T. Baumert
Institut für Physik und CINSaT, Universität Kassel,
Heinrich-Plett-Str. 40, 34132 Kassel, Germany
e-mail: wollenha@physik.uni-kassel.de

ples of PAD measurements by using laser fields of arbitrary polarization and present a method to directly reconstruct three-dimensional asymmetric wave packets from measured PADs. As an example, we study 1 + 2 Resonance Enhanced Multi-Photon Ionization (REMPI) of potassium atoms by linearly and elliptically polarized light. First, we use linear polarization in order to compare the results of the tomographic reconstruction technique with the Abel-inversion. In the case of elliptically polarized light, an Abel-inversion is no longer applicable. However, our tomographic technique still allows us to reconstruct the full three-dimensional electron wave packet.

2 Tomographic reconstruction method

In this section, we describe the tomographic reconstruction scheme adapted to our experiment. Figure 1 shows the geometric arrangement of the experiment. The laser light propagates along the z -axis. By making use of a $\lambda/4$ waveplate the polarization state of the laser pulse can be changed from linear to elliptical. With a subsequent $\lambda/2$ waveplate the pulse is rotated about the z -axis (cf. (6)). Note that the $\lambda/2$ waveplate mirrors the \mathcal{E}_y component of the field and, therefore, the main axis of the elliptically polarized light, rotated by the $\lambda/4$ waveplate, is rotated in opposite direction ($-\alpha$). The planar detector is oriented perpendicularly

to the x -axis, such that the measured photoelectron distributions are the projections $p_\theta(y, z)$ of the three-dimensional probability density of the electron wave packet $\rho_\theta(x, y, z) = |\psi_\theta(x, y, z)|^2$ (see Figs. 1(a)–(c)). Quantitatively, the projections are obtained via Abel-transform, i.e. by integration along the x -axis

$$p_\theta(y, z) = \int \rho_\theta(x, y, z) dx. \quad (1)$$

The three-dimensional wave packets are reconstructed from a set of two-dimensional projections $p_\theta(y, z)$ measured at different angles θ by making use of a Fourier-transform based tomographic technique (see for example [26]). For simplicity, we first consider a two-dimensional slice $\rho_\theta(x, y, z_0)$ through the probability density $\rho_\theta(x, y, z)$ in the x - y -plane at the position z_0 on the z -axis. The projection of this slice

$$p_\theta(y, z_0) = \int \rho_\theta(x, y, z_0) dx. \quad (2)$$

is a one-dimensional cut through the measured projection $p_\theta(y, z)$ along the y -axis. The cut positions are indicated by the thick black lines in Fig. 1(a)–(c) and the cuts $p_\theta(y, z_0)$ are represented by the corresponding reddish curves. Fourier-transform of these cuts yields

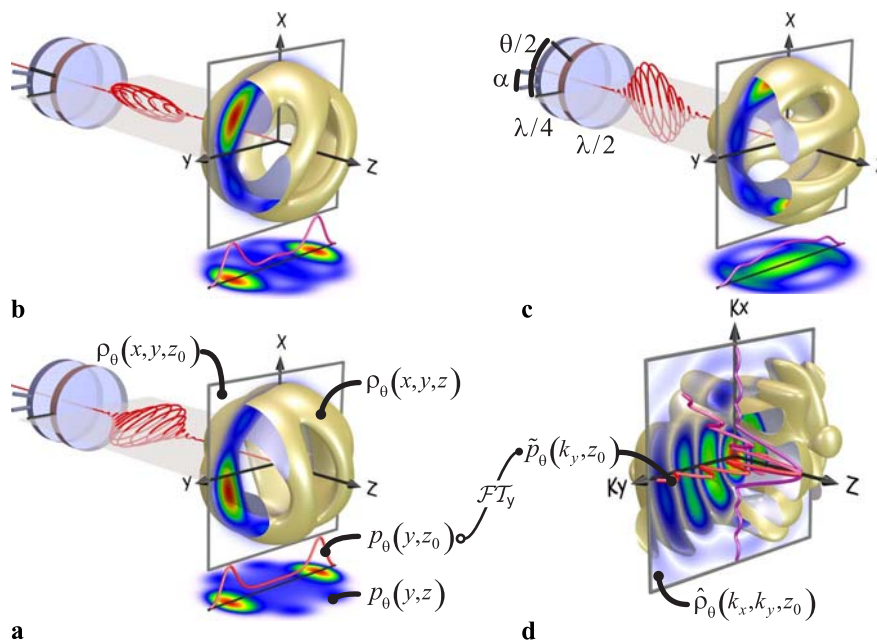


Fig. 1 Scheme of the experiment for tomographic reconstruction of the wave packet. (a)–(c) show examples of iso-surfaces (yellow) of the probability density $\rho_\theta(x, y, z)$ of the electron wave packet from 1 + 2 REMPI of potassium atoms by elliptically polarized light ($\lambda/4$ waveplate at $\alpha = 15^\circ$). The density is rotated about the z -axis by (a) $\theta = 0^\circ$, (b) $\theta = 45^\circ$ and (c) $\theta = 90^\circ$ employing a $\lambda/2$ wave-

plate at a rotation angle of $\theta/2$. The density $\rho_\theta(x, y, z_0)$ is obtained by two-dimensional Fourier-transform of the k -space distribution $\hat{\rho}_\theta(k_x, k_y, z_0)$ shown in (d). Slices through k -space are constructed by a series of one-dimensional Fourier-transforms of the projections $\mathcal{FT}_y\{p_\theta(y, z_0)\}$ measured at many different angles θ . For details see text

$$\tilde{p}_\theta(k_y, z_0) = \int p_\theta(y, z_0) e^{-ik_y y} dy. \quad (3)$$

In order to elucidate how we use the cuts $p_\theta(y, z_0)$ to reconstruct the slice $\rho_\theta(x, y, z_0)$ we consider that the two-dimensional Fourier-transform of the slice at z_0

$$\hat{\rho}_\theta(k_x, k_y, z_0) = \iint \rho_\theta(x, y, z_0) e^{-i(k_x x + k_y y)} dx dy, \quad (4)$$

yields a two-dimensional slice in k -space. It follows for $k_x = 0$

$$\hat{\rho}_\theta(0, k_y, z_0) = \iint \rho_\theta(x, y, z_0) e^{-ik_y y} dx dy = \tilde{p}_\theta(k_y, z_0) \quad (5)$$

that the one-dimensional Fourier-transform of the projection $\mathcal{FT}_y\{p_\theta(y, z_0)\}$ is the one-dimensional cut through the two-dimensional Fourier-transform $\tilde{\rho}_\theta(k_x, k_y, z_0)$ at $k_x = 0$. For visualization, we plot a curve of the one-dimensional Fourier-transform $\tilde{p}_\theta(k_y, z_0)$ at the position $k_x = 0$ on top of the two-dimensional slice in k -space $\hat{\rho}_\theta(k_x, k_y, z_0)$ (see Fig. 1(d)). As we rotate the whole distribution $\rho_\theta(x, y, z)$ about the z -axis by an angle θ and repeat the above procedure another cut through the slice $\hat{\rho}_\theta(k_x, k_y, z_0)$ at the angle θ is obtained. In Fig. 1(d) the cuts $\hat{\rho}_\theta(0, k_y, z_0) = \tilde{p}_\theta(k_y, z_0)$ through the k -space slice $\hat{\rho}_\theta(k_x, k_y, z_0)$ at different angles and their Fourier-pairs, i.e. the cuts through the respective projections $p_\theta(y, z)$, are indicated with the same colors as in Fig. 1(a)–(c). In this way, a set of cuts through the projections $p_\theta(y, z_0)$ measured at different angles θ delivers the corresponding set of cuts through the k -space slice that are used to reconstruct the full k -space slice. Subsequent two-dimensional inverse Fourier-transform of $\hat{\rho}_\theta(k_x, k_y, z_0)$ yields the slice in coordinate space $\rho_\theta(x, y, z_0)$. Repeating this procedure for the slices at different z -positions yields the full tomographic reconstruction of the probability density $\rho(x, y, z)$.

3 Experimental

In the experiment we create free electron wave packets with an average kinetic energy of 200 meV and $|f\rangle$ symmetry by 1 + 2 REMPI of potassium atoms. The experimental setup and the corresponding ionization scheme are described elsewhere in detail [25]. In brief, the setup consists of an amplified 1 kHz Ti:sapphire laser system and a photoelectron imaging spectrometer employing the Velocity-Map-Imaging (VMI) method [16]. The spectrum of our laser pulses (initially about 30 fs Full Width at Half Maximum (FWHM) with a central wavelength of 785 nm) is deliberately narrowed and shifted in a prism compressor resulting

in laser pulses of about 60 fs duration and 800 nm central wavelength, i.e. a detuning of 30 nm with respect to the K $4p \leftarrow 4s$ transition, in order to suppress the high energy component of the Autler–Townes doublet [27, 28]. The polarization state of the laser pulses is modified by using achromatic $\lambda/4$ and $\lambda/2$ waveplates (*B. Halle*). With the $\lambda/4$ waveplate at an angle α elliptically polarized pulses are produced as a prototype for polarization-shaped pulses (see Fig. 1). With the $\lambda/2$ waveplate used behind the $\lambda/4$ waveplate we rotate the polarized laser pulses about the z -axis. Note that a $\lambda/2$ waveplate at the angle of $\theta/2$ rotates *any polarization-shaped* pulse by an angle of θ since

$$\mathcal{R}(\theta/2) \cdot \mathcal{J}_{\lambda/2} \cdot \mathcal{R}^{-1}(\theta/2) \cdot \begin{pmatrix} \mathcal{E}_x(t) \\ \mathcal{E}_y(t) \end{pmatrix} = \mathcal{R}(\theta) \cdot \begin{pmatrix} \mathcal{E}_x(t) \\ -\mathcal{E}_y(t) \end{pmatrix}, \quad (6)$$

where

$$\mathcal{R}(\theta) = \begin{pmatrix} \cos(\theta) & -\sin(\theta) \\ \sin(\theta) & \cos(\theta) \end{pmatrix} \quad \text{and} \quad \mathcal{J}_{\lambda/2} = \begin{pmatrix} 1 & 0 \\ 0 & -1 \end{pmatrix} \quad (7)$$

denote a rotation matrix and a Jones-matrix for a $\lambda/2$ waveplate, respectively. This procedure is generally applicable, since the change of the sign of $\mathcal{E}_y(t)$ applies to all angles θ and therefore the shape of the pulse $\{\mathcal{E}_x(t), -\mathcal{E}_y(t)\}^T$ is preserved upon rotation. The orientation of the crystal axes of the waveplates in relation to both the laser polarization and the photoelectron imaging spectrometer was checked by using appropriate polarizers and a powermeter. The spectrally narrowed laser pulses (2.2 μJ pulse energy) were focussed into potassium vapor by an $f = 20$ cm lens, corresponding to a peak intensity of about 1.5×10^{11} W/cm² and an Autler–Townes splitting of approximately 220 meV. Photoelectrons released during the interaction of the polarized pulses with atoms were detected by the photoelectron imaging spectrometer. In the case of linearly polarized light with the polarization vector parallel to the detector, the three-dimensional angular distribution can be reconstructed from the measured PAD by Abel-inversion. Among the algorithms developed to perform the inversion [11–13, 17] we compare the results from our tomography algorithm to the distribution obtained with the pBasex-algorithm [14]. Under typical experimental conditions, we observe about 100 events from a single pulse. Measuring at a repetition rate of 1 kHz, the signal-to-noise ratio of the images is increased by using one minute time-integration of the signal in a computer yielding about 10^7 events for every projection. To obtain a high quality three-dimensional reconstruction we use up to 36 projections to cover an angle interval of 180°. Data acquisition of a full set of projections is accomplished within around 40 min.

4 Results

We studied PADs from linearly and elliptically polarized light. Linearly polarized pulses were used to produce cylindrically symmetric electron wave packets with $|f, m = 0\rangle$ symmetry where the Abel-inversion technique applies. This example served as a check of the validity of our tomographic approach. Elliptically polarized pulses generate linear combinations of multiple $|f, m\rangle$ states [25] with (1) an orientation out of the y - z -plane and (2) no cylindrical symmetry. In this case reconstruction is only possible with the tomographic technique.

Figures 2(a)–(f) show six sample PADs from excitation with linearly polarized light, i.e. $\alpha = 0^\circ$, measured at different projection angles θ . A series of 36 PADs are used for three-dimensional tomographic reconstruction of the wave packet. The upper blue surface in Fig. 2(g) is an iso-surface from the tomographically reconstructed $|f, m = 0\rangle$ wave packet. The Abel-inverted distribution (not shown) is rotated about the electrical field vector, i.e. the y -axis, to generate the red lower iso-surface. The excellent agreement between the tomographic reconstruction and the Abel-inversion con-

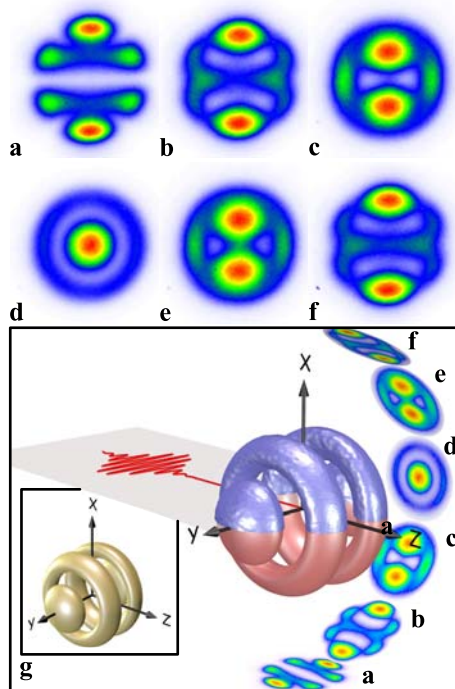


Fig. 2 (a)–(f) Measured two-dimensional photoelectron distributions $p_\theta(y, z)$ from 1 + 2 REMPI of potassium atoms with linearly polarized laser pulses at the angles $\theta = 0^\circ, 15^\circ, 30^\circ, 45^\circ, 60^\circ$ and 75° obtained by rotation of a $\lambda/2$ waveplate by $\theta/2$. (g) Result of the tomographic reconstruction of the cylindrically symmetric wave packet (upper blue iso-surface) compared to the reconstruction employing the Abel-inversion (lower red iso-surface). The inset to (g) shows an iso-surface (yellow) of a simulation of the wave packet according to [25]

firms the validity of our technique for cylindrically symmetric wave packets. The inset to Fig. 2(g) shows the result of a simulation according to [25] being in agreement with both experimental results. In order to provide the link between reconstructed density and the measured PADs (a)–(f), the latter are shown again in (g) at the respective projection angles θ . Due to the mirror symmetry of the wave packet with respect to the y - z -plane the images (b) and (f) and also (c) and (e) are geometrically equivalent and virtually identical.

Figures 3(a)–(f) show PADs measured at different projection angles θ from REMPI with elliptically polarized light obtained by rotation of the $\lambda/4$ waveplate by $\alpha = 15^\circ$. Because (1) the main axis of the polarization ellipse is out of the y - z -plane and (2) the light field has a component normal to the detector plane, this light field serves as a prototype for complex polarization-shaped pulses. Due to the selection rules for multi-photon excitation, elliptically polarized light generates linear combinations of multiple $|f, m\rangle$ states with (1) an orientation out of the y - z -plane and (2) no cylindrical symmetry. Both these properties preclude the reconstruction of this asymmetric wave packet via Abel-inversion. Therefore, the tomographic technique we propose in this contribution has to be employed for *direct* three-dimensional recon-

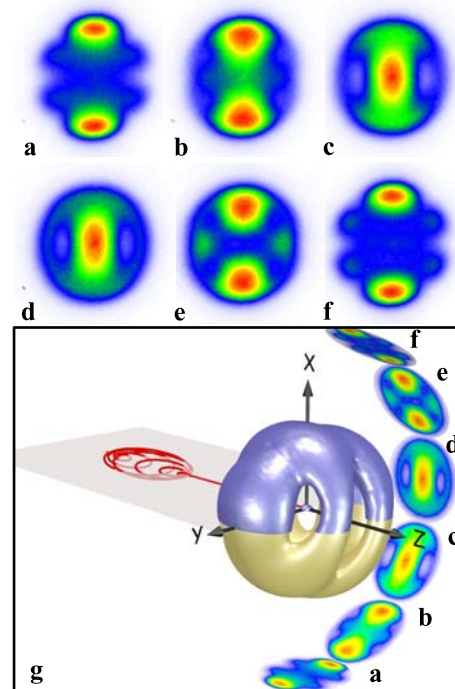


Fig. 3 (a)–(f) Measured two-dimensional photoelectron distributions $p_\theta(y, z)$ from 1 + 2 REMPI of potassium atoms with elliptically polarized laser pulses ($\lambda/4$ waveplate at 15°) at angles θ ranging from 0° to 75° . (g) Result of the tomographic reconstruction of the wave packet (upper blue iso-surface) compared to a simulation (lower yellow iso-surface). Note that this wave packet has an orientation out of the y - z -plane and shows no cylindrical symmetry. The measured distributions (a)–(f) are shown again in (g) at the respective projection angles θ

struction of the wave packet. The experimental result represented as the upper blue iso-surface in Fig. 3(g) is compared to a (scaled) simulation (yellow lower iso-surface) performed according to [25]. Due to the lack of mirror symmetry of the wave packet with respect to the y - z -plane, the projections shown in (b) and (f) as well as (c) and (e) are no longer equivalent.

5 Conclusions

In this contribution we demonstrated a novel experimental technique for accurate three-dimensional reconstruction of the shape of a free electron wave packet by generalizing beyond conventional photoelectron imaging methods. We tomographically reconstructed wave packets by measuring a series of Photoelectron Angular Distributions (PADs) at different angles with respect to the laser pulse. Employing up to 36 images for tomographic reconstruction yields highly detailed three-dimensional representations of the wave packets. Results obtained from measurements with linearly polarized light have been compared to wave packets obtained by Abel-inversion, achieving remarkable agreement. Elliptically polarized laser pulses served as prototypes for more complex polarization-shaped pulses. In this case, Abel-inversion is no longer applicable since the wave function of the ejected electron is neither oriented parallel to the detector plane nor cylindrically symmetric. A comparison to quantum mechanical simulations shows excellent agreement. Because our Fourier based tomographic reconstruction algorithm does not require any symmetry assumptions, it is well suited for reconstruction of wave packets from complex light-matter interactions and opens up fascinating routes from novel schemes for analytics to highly differential time resolved studies down to the attosecond regime. In general, the combination of three-dimensional *control* by polarization-shaped laser pulses with three-dimensional *detection* via tomographic reconstruction provides a powerful tool to exploit the three-dimensional character of light-matter interaction.

Acknowledgements The financial support by the Deutsche Forschungsgemeinschaft DFG and the EU Marie-Curie initial training network FASTQUAST is gratefully acknowledged.

References

1. A. Weiner, Rev. Sci. Instrum. **71**, 1929 (2000)
2. M. Wollenhaupt, A. Assion, T. Baumert, in *Springer Handbook of Lasers and Optics* (Springer, Berlin, 2007)
3. T. Brixner, G. Krampert, T. Pfeifer, R. Selle, G. Gerber, M. Wollenhaupt, O. Graefe, C. Horn, D. Liese, T. Baumert, Phys. Rev. Lett. **92**, 208301 (2004)
4. N. Dudovich, D. Oron, Y. Silberberg, Phys. Rev. Lett. **92**, 103003 (2004)
5. T. Suzuki, S. Minemoto, T. Kanai, H. Sakai, Phys. Rev. Lett. **92**, 133005 (2004)
6. M. Wollenhaupt, V. Engel, T. Baumert, Annu. Rev. Phys. Chem. **56**, 25 (2005)
7. M. Wollenhaupt, A. Assion, D. Liese, C. Sarpe-Tudoran, T. Baumert, S. Zamith, M. Bouchene, B. Girard, A. Flettner, U. Weichmann, G. Gerber, Phys. Rev. Lett. **89**, 173001 (2002)
8. T. Brixner, G. Gerber, Opt. Lett. **26**, 557 (2001)
9. see e.g. J. Ullrich, R. Moshhammer, A. Dorn, R. Dörner, L. Schmidt, H. Schmidt-Böcking, Rep. Prog. Phys. **66**, 1463 (2003) and references therein
10. J. Itatani, J. Levesque, D. Zeidler, H. Nikura, H. Pépin, J. Kieffer, P. Corkum, D. Villeneuve, Nature **432**, 867 (2004)
11. C. Bordas, F. Paulig, H. Helm, D. Huestis, Rev. Sci. Instrum. **67**, 2257 (1996)
12. M. Vrakking, Rev. Sci. Instrum. **72**, 4084 (2001)
13. V. Dribinski, A. Ossadtchi, V. Mandelshtam, H. Reisler, Rev. Sci. Instrum. **73**, 2634 (2002)
14. G. Garcia, L. Nahon, I. Powis, Rev. Sci. Instrum. **75**, 4989 (2004)
15. D. Chandler, P. Houston, J. Chem. Phys. **87**, 1445 (1987)
16. A. Eppink, D. Parker, Rev. Sci. Instrum. **68**, 3477 (1997)
17. J. Winterhalter, D. Maier, J. Honerkamp, V. Schyja, H. Helm, J. Chem. Phys. **110**, 11187 (1999)
18. B. Whitaker, *Imaging in Molecular Dynamics* (Cambridge University Press, Cambridge, 2003)
19. M. Wollenhaupt, A. Assion, O. Bazhan, C. Horn, D. Liese, C. Sarpe-Tudoran, M. Winter, T. Baumert, Phys. Rev. A **68**, 015401 (2003)
20. N. Dudovich, T. Polack, A. Pe'er, Y. Silberberg, Phys. Rev. Lett. **94**, 083002 (2005)
21. M. Wollenhaupt, D. Liese, A. Präkelt, C. Sarpe-Tudoran, T. Baumert, Chem. Phys. Lett. **419**, 184 (2006)
22. C. Trallero-Herrero, J. Cohen, T. Weinacht, Phys. Rev. Lett. **96**, 063603 (2006)
23. E. Shapiro, V. Milner, C. Menzel-Jones, M. Shapiro, Phys. Rev. Lett. **99**, 033002 (2007)
24. T. Bayer, M. Wollenhaupt, C. Sarpe-Tudoran, T. Baumert, Phys. Rev. Lett. **102**, 023004 (2009)
25. M. Wollenhaupt, M. Krug, J. Köhler, T. Bayer, C. Sarpe-Tudoran, T. Baumert, Appl. Phys. B **95**, 245 (2009)
26. A. Kak, M. Slaney, *Principles of Computerized Tomographic Imaging* (IEEE Press, New York, 1988)
27. M. Wollenhaupt, A. Präkelt, C. Sarpe-Tudoran, D. Liese, T. Baumert, Appl. Phys. B **82**, 183 (2006)
28. T. Bayer, M. Wollenhaupt, T. Baumert, J. Phys. B **41**, 074007 (2008)